Identification and *in vitro* evaluation of new leads as selective and competitive glycogen synthase kinase-3β inhibitors through ligand and structure based drug design

B.S. Darshit [a], B. Balaji [a], P. Rani [b], M. Ramanathan [a,*]

[a] *Department of Pharmacology, PSG College of Pharmacy, Coimbatore 641004, Tamil Nadu, India*
[b] *Department of Biotechnology, PSG College of Technology, Coimbatore 641004, Tamil Nadu, India*

ABSTRACT

Glycogen synthase kinase-3β elicits multi-functional effects on intracellular signaling pathways, thereby making the kinase a therapeutic target in multiple pathologies. Hence, it is important to selectively inhibit GSK-3β over structurally and biologically similar targets, such as CDK5. The current study was designed to identify and evaluate novel ATP-competitive GSK-3β inhibitors. The study was designed to identify new leads by ligand based drug design, structure based drug design and *in vitro* evaluation. The best validated pharmacophore model (AADRRR) identified using LBDD was derived from a dataset of 135 molecules. There were 357 primary hits within the SPECS database using this pharmacophore model. A SBDD approach to the GSK-3β and CDK5 proteins was applied to all primary hits, and 5 selective inhibitors were identified for GSK-3β. GSK-3β and CDK5 *in vitro* kinase inhibition assays were performed with these molecules to confirm their selectivity for GSK-3β. The molecules showed IC_{50} values ranging from 0.825 μM to 1.116 μM and were 23- to 57-fold selective for GSK-3β. Of all the molecules, molecule 3 had the lowest IC_{50} value of 0.825 μM. Our research identified molecules possessing benzothiophene, isoquinoline, thiazolidinedione imidazo-isoquinoline and quinazolinone scaffolds. Potency of these molecules may be due to H-bond interaction with backbone residues of Val135, Asp133 and side chain interaction with Tyr134. Selectivity over CDK5 may be due to side chain interactions with Asp200, backbone of Val61, ionic interaction with Lys60 and π-cationic interaction with Arg141. These selective molecules were also exhibited small atom hydrophobicity and H-bond interaction with water molecule.

© 2014 Elsevier Inc. All rights reserved.

1. Introduction

Glycogen synthase kinase-3 (GSK-3) is a highly conserved proline-directed serine/threonine protein kinase. Two isoforms of GSK-3, GSK-3α (51 kDa) and GSK-3β (47 kDa), possess identical sequences in their protein kinase domains [1]. Both proteins are distributed and widely expressed throughout the body and are mainly present in growing axons, dendrites and in the nuclei of neurons during transcriptional processes [2,3]. These proteins have a long half-life, and their post-translational modification is preferentially regulated by protein–protein interactions. The regulation of various signaling pathways is affected by the phosphorylation pattern of GSK-3β. The activation and inhibition of GSK-3β is regulated by the phosphorylation of Tyr216 and Ser9, respectively [4].

Various upstream substrates control the phosphorylation states of these two amino acid residues, thereby regulating the post-translational modification and downstream signaling of GSK-3β. Several proteins are substrates that regulate GSK-3β function. GSK-3β accepts these substrates in its phosphorylated state [5]. GSK-3β activity has therapeutic implications in several pathologies, such as Alzheimer's disease, Parkinson's disease, ischemic stroke, mood disorders, inflammation, diabetes mellitus and cancer [6]. Apart from the above-mentioned clinical conditions, GSK-3β is also part of cell regulatory signaling pathways, the predominant of these being cell fate, insulin and *Wnt* signaling.

GSK-3β protein has structural homology to other proteins, such as extracellular receptor kinase (ERK) and members of the cyclin-dependent protein kinase (CDK) family, especially CDK2 and CDK5 [7]. Among these targets, CDK5 has controversial functions and interferes with the downstream response of GSK-3β. Of all the CDKs, CDK5 has neuronal cell-specific functioning [8], apart from its involvement in cell cycle regulation. Neuronal migration and differentiation are important processes that can be regulated by CDK5

* Corresponding author. Tel.: +91 422 2570 170; fax: +91 422 259 4400.
 E-mail addresses: muthiah.in@gmail.com, muthiahramanathanin@yahoo.co.in
(M. Ramanathan).

Dataset created from literature – 135 molecules

Pharmacophore model (AADRRR) selected from highly potent molecules
(Ligand based approach)

Screening of SPECS database through validated pharmacophore model (> 200,000 molecule)

Retrieval of primary hits (357 molecules)

Docking of these primary hits with GSK-3β and CDK5 protein
(Structure based approach)

Selection of molecules (5 molecules)

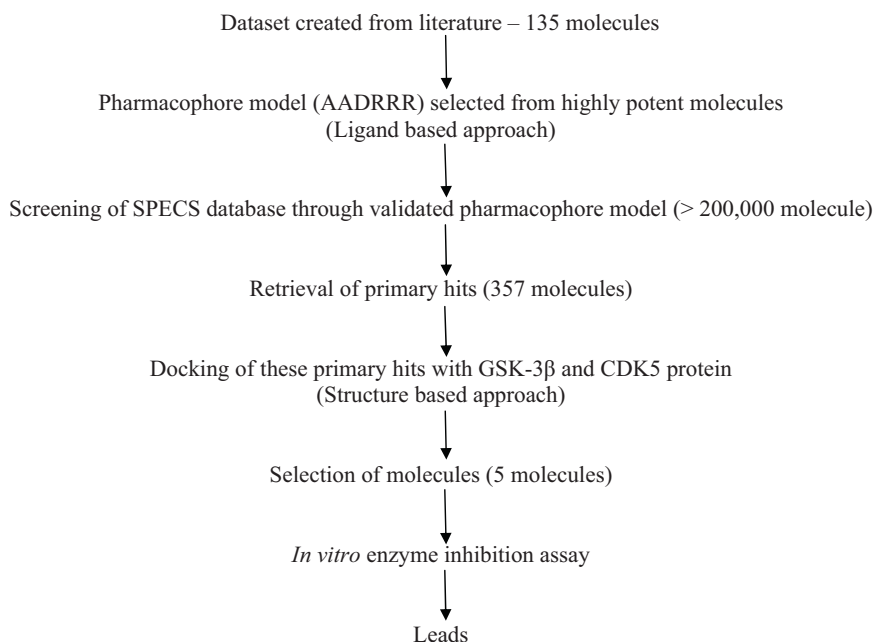*In vitro* enzyme inhibition assay

Leads

Fig. 1. A flow chart showing the lead identification protocol.

after the mitotic phase of the cell cycle [9–11]. This homology and interference in biological activity encourage the identification of inhibitors that are selective for GSK-3β over CDK5.

The inhibition of GSK-3β by lithium [12] has highlighted the importance of GSK-3β in mental and psychiatric disorders. Following this hypothesis, several molecular chemotypes have been developed, such as hymenialdisine, paullone, aminopyridine, indirubin, maleamide, pyrazolo-pyridazine, oxadiazole, sulfonamide, benzazepinone, bis-indole and pyrazolopyridine [13]. All of the above chemotypes are ATP competitors and have been shown to inhibit GSK-3β activity. However, a major disadvantage of these molecules is their lack of selectivity for GSK-3β over other homologous kinases within in the biological system. Other molecules have exhibited non-ATP-competitive inhibition, such as thiadiazolidinedione derivatives [14], menzamine [15], thienyl and phenyl α-halomethyl ketones molecules [16]. These molecules bind to the non-ATP competitive prime site of the GSK-3β. The advantage of these molecules is their selectivity, which decreases their possible side effects.

There are several molecules with different scaffolds, being studied in clinical trials are listed here with. SB-216763 and SB-41528, maleimide derivatives (SmithKline Beecham pharmaceuticals), the aminopyridine derivatives CHIR98023 and CHIR99021 (Chiron Corporation), the aminothiazole derivative AR-A 014418 (AstraZeneca), the maleimide derivative LY-317615 (Enzastaurin, Eli Lilly & Co), NP-12, the thiadiazolidinedione derivative NP-031112 (Neuropharma SA, Zeltia SA), Neu-120 (Neurim Pharmaceuticals), CP-70949 (Pfizer Inc.), SAR-502250 (Sanofi-Aventis), VX-608 (Vertex Pharmaceuticals Inc.), and KUSTU-144 – cazpaullone (DeveloGen AG) are also being evaluated as GSK-3β inhibitors in different pathological conditions [17]. Currently, many researchers are working on developing new GSK-3β-targeting chemical entities with reduced selectivity issues.

The ligand-based approach is by far the most applied technique in the initial phase of drug discovery. Crystallographic protein structures offer valuable information about important interactions, bioactive ligand conformations and ligand geometry within the binding grooves of proteins. Discovering three-dimensional pharmacophores that explain the activity of a series of ligands is one of the most significant contributions of computational chemistry

to drug discovery. A good pharmacophore model collects important common features of molecules distributed in 3D space and provides a rational hypothetical 3D model of the primary chemical features responsible for activity. Such 3D models are more easily interpretable than 2D descriptor or fingerprint-based QSAR models, making it easier to suggest new compounds for synthesis. Consequently, pharmacophore study has become an important method and has proven extremely successful not only in demonstrating structure–activity relationships but also in developing new drugs [18]. The synergy of molecular docking and pharmacophore generation can produce reliable results in subsequent virtual screening [19]. The virtual screening flow chart is shown in Fig. 1.

The objective of the present study is to find selective GSK-3β inhibitors possessing new scaffolds through ligand- and structure-based drug design and to confirm the activities of the hits using an *in vitro* assay of GSK-3β inhibition. Molecules were also screened for CDK5 enzyme inhibition to determine their selectivity for GSK-3β. Ligand-based drug design was employed to extract a pharmacophore model. This pharmacophore model was then used to screen the SPECS database to identify primary hits. The potential GSK-3β-selective inhibitors among the primary hits were selected through structure-based drug design, and their activity was confirmed using a kinase inhibition assay.

2. Methodology

2.1. Computational details

2.1.1. Dataset for analysis

There were 135 molecules selected from 3 different scaffolds: N-phenyl-4-pyrazolo[1,5-b]pyridazine-3-yl pyrimidine-2-amines (71 molecules) [20], indirubins (33 molecules) [21] and 2-{3-[4-(alkylsulfinyl)phenyl]-1-benzofuran-5-yl}-5-methyl-1,3,4-oxadiazoles (31 molecules) [22]. These molecules are reported to have activities ranging from 0.3 nM to 31.6 μM. Molecules were selected whose QPLogP value > 1. All active molecules that were considered for pharmacophore generation have shown QPLogP > 2 that ensures good cellular and brain permeability. Also these 8 active molecules that were selected had cellular

$EC_{50} < 2\,\mu M$. Molecules were included which displayed 2- to 2000-folds selective toward GSK-3β. Those molecules whose activities were not exactly mentioned were discarded from this study. To carry out the structure- and ligand-based drug design process, IC_{50} values for the molecules were converted to a logarithmic scale.

2.1.2. Ligand preparation

All 135 molecules were built in Maestro, Schrödinger [23]. The LigPrep module of Schrödinger [24] was used to clean the structure by converting 2D structure to 3D, minimizing the energy state of molecule, adding missing hydrogens, generating stereoisomers, neutralizing charged structures, and determining possible ionization at a defined pH of 7.2 ± 2. Due to the pharmacokinetic aspect, ligands were prepared in a pH range of 5.2–9.2. This pH range led protonation of certain molecules that was considered in pharmacophore generation. The conformational space was explored through a combination of Monte-Carlo Multiple Minimum (MCMM) and Low Mode (LMOD) with a maximum number of 1000 conformers per structure and 100 minimization steps. Each minimized conformer was filtered through a relative energy window of $10\,kJ\,mol^{-1}$ and a minimum atomic deviation of $1.00\,\text{Å}$. An energy value of $10\,kJ\,mol^{-1}$ set an energy threshold relative to the lowest-energy conformer. Conformers that had energies higher than this threshold were discarded. For two conformers to be considered identical, all distances between the pairs of corresponding heavy atoms were required to be less than $1.00\,\text{Å}$ [25,26].

2.1.3. 3D QSAR studies

In the present study, the PHASE module of Schrödinger [27] was used for 3D QSAR pharmacophore model development. PHASE is a highly flexible system for pharmacophore perception, structure alignment, activity prediction, and 3D database searching. PHASE identifies pharmacophores that are common to a set of actives in 3D space using different sites. Each ligand structure is represented by a set of points in 3D space, which coincides with various chemical features that may facilitate noncovalent binding between the compound and its target receptor. PHASE provides a built-in set of six pharmacophore features: hydrogen bond acceptors (A), hydrogen bond donors (D), hydrophobic groups (H), negatively ionizable groups (N), positively ionizable groups (P), aromatic rings (R) and custom features (X, Y, Z).

Entire dataset of ligands was divided into active and inactive classes using threshold pIC_{50} values of 8.5 and 6.5, respectively, resulting in 8 active and 33 inactive molecules. These active and inactive molecules were used for pharmacophore hypothesis generation and subsequent scoring. Hypotheses were generated by a systematic variation of the number of sites (n_{sites}) and the number of matching active compounds (n_{act}). Initially, the number of sites was varied by keeping all active molecules until at least one hypothesis was found and scored successfully. The common pharmacophore hypothesis must match the common pharmacophore sites of all the actives. Common pharmacophores were perceived using a tree-based partitioning technique that groups together similar pharmacophores according to their intersite distances. Thus, a k-point pharmacophore is represented by a vector of n distances, where $n = k(k-1)/2$. Each intersite distance (d) was filtered through a binary decision tree. All pharmacophores of a given variant that mapped into the same terminal box were considered to be similar enough to facilitate the identification of a common pharmacophore. Default parameters such as volume, site, vector, selectivity, number of matches and energy terms were used to score the hypothesis. The process of scoring with respect to actives molecules was designed to filter out inappropriate pharmacophores and to identify within each box a top ranked representative, henceforth referred to as the pharmacophore hypothesis for that box. At that point, only information from the actives was used. Each pharmacophore from a

surviving box was treated temporarily as a reference to assign a score. Accordingly, all other non-reference pharmacophores from that box and its neighboring boxes were aligned, one-by-one, to the reference pharmacophore, and the quality of the alignments was measured using two criteria: RMSD in the pharmacophore site point positions and the average cosine of the angles formed by corresponding pairs of vector features.

For the evaluation of the hypotheses, the training and test set molecules were kept constant. The dataset was randomly divided at a 1:1 ratio into a training set and a test set with most inactive and active molecules belongs to the training set. Based on scoring, top 10% hypotheses were considered for the generation of QSAR model. Among these hypotheses, the best one hypothesis was selected for screening of database.

In these 3D QSAR models, chemical features of ligand structures were mapped to a cubic 3D grid. The pharmacophoric model used a grid spacing of $1\,\text{Å}$. All the common pharmacophore hypotheses were successfully generated and scored by correlating the observed and estimated activities for the training set molecules using partial least squares (PLS) analysis. Cross validation analysis was performed to evaluate the model by leave multiple out (leave 20% out) method. The maximum number of usable PLS factors was $N/5$, where N was the number of ligands in the training set, as using larger numbers of PLS factors led to the over-fitting of the data [28].

2.1.4. Database searching

A pharmacophore validated by scoring and statistics was used to find hits from the SPECS database (http://www.specs.net/snpage.php?snpageid=home). SPECS database is widely utilized in drug discovery process. There are over 200,000 molecules existing in database and used to find hits. Chemical space and descriptor distribution of these molecules is shown in supplementary data, Figure S1. PHASE performs two steps for hit searching: finding followed by fetching. PHASE searches database using sites and geometric arrangements to find molecules that match the hypothesis and then retrieve the relevant conformers from the database for alignment to the hypothesis.

2.1.5. Docking studies

A pharmacophore model was generated from the dataset, validated and then used to screen the SPECS database. Molecules screened through a common pharmacophore were isolated, and ligand preparation was performed for further docking analysis. For structure based approach, GSK-3β (PDB ID: 1Q5K) [29] and CDK5 (PDB ID: 1UNL) [30] crystal structures, co-crystallized with AR-A 014418 and R-roscovitine respectively, were used. These protein crystal structures were downloaded from protein databank (RCSB PDB: http://www.rcsb.org/pdb/home/home.do). GSK-3β crystal structures were classified into three major groups based on the conformational changes of Gln185 [29]. Among these three groups, 1Q5K co-crystallized with AR-A 014418 was utilized because of high resolution ($1.94\,\text{Å}$) and its wide utility for docking studies. Simultaneously, for CDK5/p25 protein, 1UNL crystal structure co-crystallized with R-roscovitine was used having resolution of $2.20\,\text{Å}$.

The purpose of using CDK5 protein was to identify the selectivity of the molecules toward GSK-3β by means of docking score and interactions. Before performing docking analysis, the proteins were validated in terms of ATP binding site, interactions and RMSD value. In order to confirm the ATP binding site in the protein, ATP was docked to both proteins, and interactions were observed. Based on the interaction of ATP and the reference standard with GSK-3β and CDK5 proteins key amino acid residues were selected to identify molecules. Root mean square deviation (RMSD) was calculated between the native X-ray crystal and best docked pose of the

Table 1

Representing the dataset molecules used to generate the pharmacophore model showing their observed and predicted log IC$_{50}$ values. These datasets include (1) N-phenyl-4-pyrazolo[1,5-b]pyridazine-3-yl pyrimidine-2-amines derivatives; (2) indirubin derivatives; (3) 2-{3-[4-(alkylsulfinyl)phenyl]-1-benzofuran-5-yl}-5-methyl-1,3,4-oxadiazole derivatives.
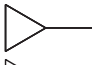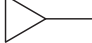
1. N-Phenyl-4-pyrazolo[1,5-b]pyridazine-3-yl pyrimidine-2-amines derivatives

No.	Y	R	R$_6$	B	R$_2$	R$_5$	Log IC$_{50}$	pLog IC$_{50}$
1[a]	H	H					7.7212	7.979
2	H	Me					4.7011	6.718
3[a,b]	2-Me	H					5.2218	–
4[a]	3-OMe	H					8	8.107
5[a]	4-CN	H					8.6989	8.219
6	4-NO$_2$	H					8.6989	8.044
7[a]	4-CH(CH$_3$)$_2$	H					7.5086	7.698
8	4-CH(C$_2$H$_5$)(CH$_3$)	H					6.9030	7.723
9	4-C(CH$_3$)$_3$	H					7.3010	7.683
10	3-OMe, 4-OMe	H					7.9208	8.112
11	3-F, 4-F	H					8	8.205
12	3-Cl, 4-Cl	H					8	8.209
13	3-CF$_3$, 4-Cl	H					8.6989	8.264
14[a]	3-OMe, 5-OMe	H					7.9208	8.324
15[a]	3-OMe, 5-CF$_3$	H					8.6989	8.923
16[a]	3-Br, 5-CF$_3$	H					9.5228	9.253
17[a]	3-F, 5-F	H					8.6989	8.745
18	3-Cl, 5-Cl	H					9	8.83
19	3-Me, 5-Me	H					9	8.799
20[a]	3-CF$_3$		OH				7.7958	7.203
21	3-CF$_3$		OMe				7.3010	6.787
22	3-CF$_3$		OC$_2$H$_5$				6.7011	6.46
23[a]	3-CF$_3$		OC$_3$H$_7$				6.1001	6.328
24	3-OMe		OMe				7	6.785
25[a]	3-OCF$_3$		OMe				7.3010	6.875
26	4-CN		OMe				7.3010	6.789
27	4-NO$_2$		OMe				7.1023	6.738
28[a]	3-OMe, 5-OMe		OMe				6.9030	6.644
29[a]	3-OMe, 5-CF$_3$		OMe				6.7011	6.81
30	3-OMe, 5-CF$_3$		OC$_2$H$_5$				5.5000	6.777
31	3-CF$_3$, 5-CF$_3$		OMe				6.2006	6.921
32[a]	3-CF$_3$		Me				8	7.473
33[a]	4-CF$_3$		Me				7.301	7.452
34	3-OMe, 5-CF$_3$		Me				8	7.25
35	3-CF$_3$		Ph				6.8013	7.523
36[a]	H		H	H			8	7.858
37[a,b]	3-CF$_3$		H	H			7.9208	–
38	3-F, 4-F		H	H			8	7.876
39	3-F, 5-F		H	H			7.9586	7.879
40	3-CF$_3$, 4-Cl		H	H			7.6989	7.899
41[a]	H		H	4-F			7.6989	7.785
42[a]	3-CF$_3$		H	4-F			7.6989	7.162
43	3-F, 4-F		H	4-F			7.6020	6.549
44[a]	3-CF$_3$, 4-Cl		H	4-F			7.3979	6.636
45	H		H	4-OMe			5.3001	5.943
46[a]	3-CF$_3$		H	4-OMe			4.5003	4.938
47	3-F, 4-F		H	4-OMe			5.1001	5.878
48	3-CF$_3$, 4-Cl		H	4-OMe			4.5003	5.721
49[a]	H		H	3-CF$_3$			6.8013	6.408
50	3-F, 4-F		H	3-CF$_3$			6.5003	6.392
51	3-CF$_3$, 4-Cl		H	3-CF$_3$			6	6.468
52	H		H	4-Cl			5.9030	6.527
53[a]	3-CF$_3$		H	4-Cl			5.6003	6.211
54[a]	3-F, 4-F		H	4-Cl			6	6.512
55[a,b]	3-CF$_3$, 4-Cl		H	4-Cl			5.4001	–
56[a]	H		Me	H			7.3010	7.099
57	3-CF$_3$		Me	H			7.3979	7.02
58[a]	3-F, 4-F		Me	H			7.5086	6.991
59[a]	3-CF$_3$, 4-Cl		Me	H			7	7.117
60	H		Me	3-CF$_3$			6.1001	6.921
61[a]	3-F, 4-F		Me	3-CF$_3$			5.8013	6.744
62[a]	3-CF$_3$, 4-Cl		Me	3-CF$_3$			6.2006	6.87
63[a]	H		Me	4-F			7.6020	7.157
64	3-CF$_3$		Me	4-F			7.6020	7.04
65	3-F, 4-F		Me	4-F			7.7958	6.945
66	3-CF$_3$, 4-Cl		Me	4-F			7.3010	7.112
67[a]	H				H		4.7212	4.47
68[a]	3-F, 4-F				H		4.6382	4.431

Table 1 (*Continued*).
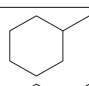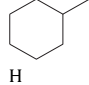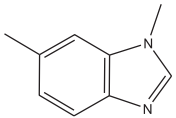
1. N-Phenyl-4-pyrazolo[1,5-b]pyridazine-3-yl pyrimidine-2-amines derivatives

No.	Y	R	R_6	B	R_2	R_5	Log IC_{50}	pLog IC_{50}
69[a]	H				H		4.7000	4.436
70	3-F, 4-F				H		4.7000	4.354
71	3-OMe				O(CH$_2$)$_2$OMe	H	7.0969	5.864

2. Indirubin derivatives

No.	X	Y	Z	W	L	R	Log IC_{50}	pLog IC_{50}
72[a]	H	O	H	H	H	H	6	6.54
73[a]	H	NOH	H	H	H	H	7.6575	6.91
74[a]	H	NOAc	H	H	H	H	6.6989	6.68
75	H	NOCH$_3$	H	H	H	H	6.8239	6.75
76	Br	O	Br	H	H	H	5.3467	6.925
77[a]	Br	NOH	Br	H	H	H	6.9208	6.791
78	H	O	Br	H	H	H	4.6575	4.079
79[a]	H	NOH	Br	H	H	H	6.4685	6.752
80	Br	O	H	H	H	H	7.3467	6.971
81	Br	NOH	H	H	H	H	8.3010	6.523
82[a]	Br	NOAc	H	H	H	H	8	7.842
83	Br	NOCH$_3$	H	H	H	H	7.5228	7.295
84[a]	Cl	O	H	H	H	H	6.8538	7.098
85[a]	Cl	NOH	H	H	H	H	7.6989	7.086
86	Cl	NOAc	H	H	H	H	7.7695	7.966
87[a]	I	O	H	H	H	H	7.2596	7.224
88	I	NOH	H	H	H	H	8	7.101
89	I	NOAc	H	H	H	H	7.8860	7.386
90[a]	CH=CH$_2$	O	H	H	H	H	6.6197	7.515
91[a]	CH=CH$_2$	NOH	H	H	H	H	7.2218	7.22
92[a]	CH=CH$_2$	NOAc	H	H	H	H	7.1870	7.234
93	F	O	H	H	H	H	6.1870	7.48
94	F	NOH	H	H	H	H	6.8860	7.282
95	F	NOAc	H	H	H	H	7.0457	7.884
96[a]	Br	O	H	CH$_3$	H	H	7.6020	8.07
97	Br	NOH	H	CH$_3$	H	H	8.2218	7.997
98[a]	Br	NOAc	H	CH$_{3a}$	H	H	8.1549	8.291
99	Cl	O	H	Cl	H	H	7.5228	8.074
100[a]	Cl	NOH	H	Cl	H	H	8.3979	7.921
101	Cl	NOAc	H	Cl	H	H	8.3979	8.174
102	Br	O	H	NO$_2$	H	H	7	8.092
103[a]	Br	NOH	H	NO$_2$	H	H	8.1549	8.675
104[a]	Br	NOAc	H	NO$_2$	H	H	8.2218	7.56

3. 2-{3-[4-(Alkylsulfinyl)phenyl]-1-benzofuran-5-yl}-5-methyl-1,3,4-oxadiazole derivatives

No.	R	Het	Ar	R′	Log IC_{50}	pLog IC_{50}
105	Ph-4-OMe				7.2676	7.36
106[a]	Ph-4-COOH				7.3010	7.967
107	Ph-4-CONH$_2$				7.1611	7.262
108[a]	Ph-4-OH				6.7447	7.026
109[a]	Ph-4-COMe				7	6.788
110	Ph-4-C(OH)Me				6.7958	6.702
111	Ph-4-COOMe				6.6989	6.903
112[a]	Ph-4-P(O)(OMe)$_2$				6.5528	6.83
113	Ph-4-F				6.9586	7.147
114[a]	Ph-4-SMe				7.1804	7.802
115	Ph-4-S(O)Me				7.4559	6.925
116[a]	Ph-4-(O)$_2$Me				7.3767	7.192
117	Ph-4-S(O)Et				7.4559	7.16
118[a]	Ph-4-S(O)$_2$Et				7.4202	7.278
119[a]	4-Py				7.1135	7.102
120	Ph-3-OMe				7.1307	6.982
121[a]	Ph-3-S(O)Me				6.6777	6.952
122					6.6989	6.804

Table 1 (*Continued*).

3. 2-{3-[4-(Alkylsulfinyl)phenyl]-1-benzofuran-5-yl}-5-methyl-1,3,4-oxadiazole derivatives

No.	R	Het	Ar	R'	Log IC$_{50}$	pLog IC$_{50}$
123[a]					6.1023	6.271
124					6	6.377
125					6.5686	6.525
126[a]					6	6.368
127					6	6.744
128[a]					7.1426	7.481
129[a]					7.0915	7.158
130					6	7.11
131					6.1674	6.892
132[a]					6	6.428
133[a]				SH	7.0268	6.958
134[a]				OH	6.8860	6.344
135				NH$_2$	7.8860	6.896

[a] Denotes the compounds included in training set and rest were in test set.
[b] Denotes an outlier molecules from training dataset.

reference standard to validate the protein crystal structures. The RMSD calculation was performed during docking run. Initially proteins and reference standard molecules were prepared separately through protein preparation wizard and LigPrep modules respectively. Grid files were generated from the prepared proteins as the reference standard molecules were considered as a centroid. Up on docking run protein grid was exported and reference ligand prepared was used in the core tab to compute RMSD through glide module. All atoms were selected in reference standard for RMSD calculation.

Crystal structure of GSK-3β and CDK5 were prepared using Protein Preparation Wizard of Maestro. Pre process was done to protein, identical chain was removed and water molecules were eliminated except those which were 5 Å surrounding to the hetero atom in active binding site. Different protonation states using a pH value of 7.2 ± 0.2 and tautomers were generated. This pH was selected as proteins are performing its physiological functioning at a physiological pH of 7.2. Docking treats the ligands with a fully flexible all-atom representation and the receptor with a rigid grid depiction. The grid was generated by applying a Van der Waals radii

scaling factor of 1.00 with a partial charge cut-off of less than 0.25. The co-crystal ligand was used to center docking box with a size capable of accommodating ligands with a length of ≤20 Å.

The docking was performed using the XP mode of the Glide module of Schrödinger [31]. Glide uses a hierarchical series of filters to search for possible locations of the ligand in the active-site region of the enzyme. The initial filters test the spatial fit of the ligand to the defined active site, and examine the complementarily of ligand–enzyme interactions using a grid-based method. Conformations that pass these initial screens enter the final stage of the algorithm, which involves evaluation and minimization of a grid approximation to the nonbonded ligand–receptor interaction energy. Final scoring was then carried out on the energy-minimized conformations and rescored using Schrödinger's proprietary GlideScore (GScore) scoring function.

2.2. In vitro kinase inhibition assay

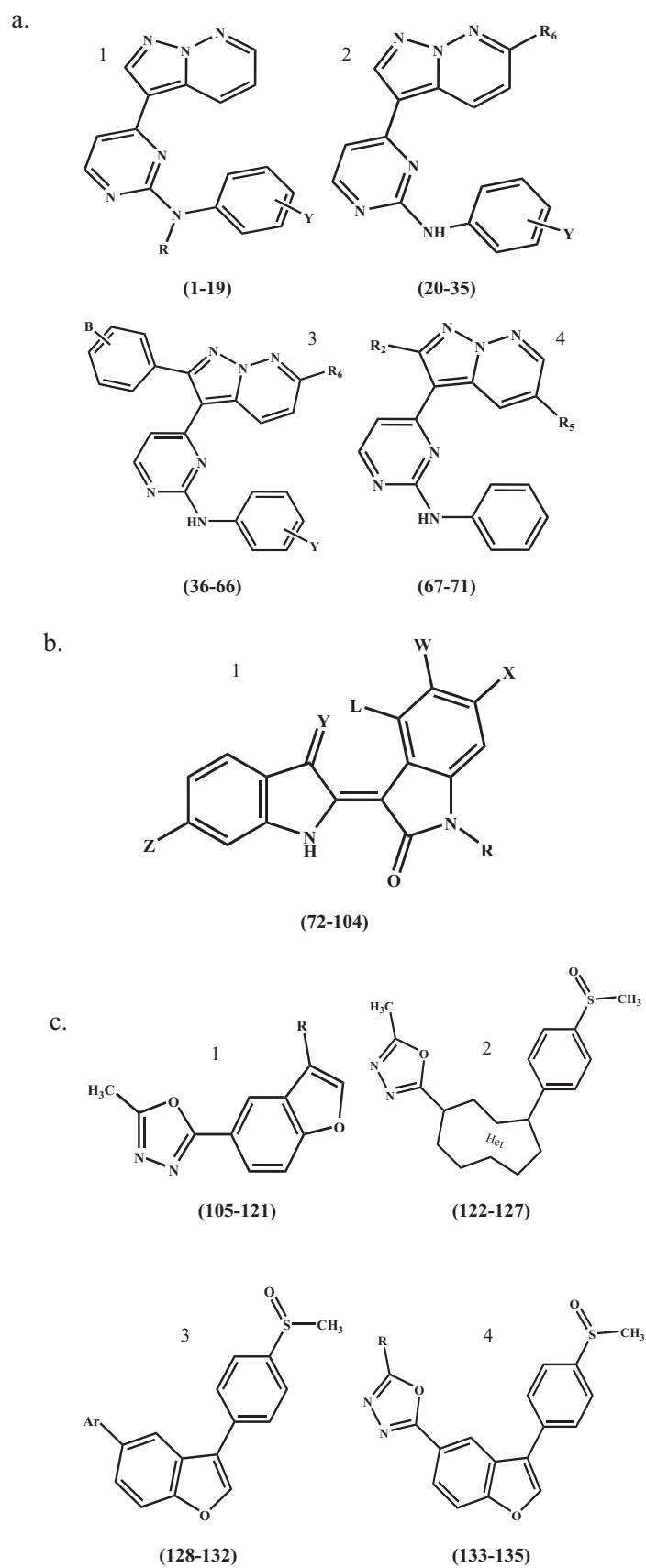The kinase assay was performed using a homogenous, non-radioactive luminescent assay [32]. Human GSK-3β enzyme,

Fig. 2. The basic structures of three different scaffolds of N-phenyl-4-pyrazolo[1,5-b]pyridazine-3-yl pyrimidine-2-amines (a), indirubin derivatives (b) and 2-{3-[4-(alkylsulfinyl)phenyl]-1-benzofuran-5-yl}-5-methyl-1,3,4-oxadiazole derivatives (c). Figure a1 (compounds 1–19), Figure a2 (compounds 20–35), Figure a3 (compounds 36–66) and Figure a4 (compounds 67–71). Figure b1 (compounds 72–104). Figure c1 (compounds 105–121), Figure c2 (compounds 122–127), Figure c3 (compounds 128–132) and Figure c4 (compounds 133–135).

glycogen synthase, which is a phosphorylated substrate of GSK-3β, and histone H1, which is a substrate of CDK5/p25 were purchased from SignalChem Life Sciences Corporation. Human CDK5/p25 enzyme was purchased from Merck Millipore (Darmstadt, Germany). Kinase-Glo reagent was purchased from Promega Corporation. Remaining buffer components, such as HEPES, EDTA, EGTA and magnesium chloride, were purchased from Sigma–Aldrich (St. Louis, MO, USA).

The final reaction buffer for the kinase assay contained 50 mM HEPES (pH 7.5), 1 mM EDTA, 1 mM EGTA, and 15 mM magnesium chloride. Test compounds were dissolved in DMSO, and the final required concentrations were achieved in the reaction mixture with assay buffer. The reaction volume (20 μl) contained 20 ng (20 nM of GSK-3β and 30 nM of CDK5/p25) of enzyme, 25 μM substrate and 1 μM ATP with and without test compound at different concentrations. The concentration of DMSO in the reaction mixture did not exceed 1%. The final reaction mixture was incubated for 30 min at 30 °C. After incubation, Kinase-Glo reagent was added to the reaction mixture to stop the kinetic reaction and further incubated for 10 min incubation. Luminescence was measured using at multimode reader immediately after 10-min incubation. A reading without test compound and with 1 μM ATP was used to define 100% activity. The Z-factor was calculated to determine the validity of the assay. The assay was performed in a solid black flat-bottom 96-well plate. The 50% inhibitory concentration (IC$_{50}$) values were calculated using GraphPad Prism 4.0 software (GraphPad software, Inc., La Jolla, CA, USA).

3. Results and discussion

3.1. Pharmacophore modeling

Pharmacophore modeling and 3D database searching are essential processes for lead discovery and optimization. PHASE identifies spatial arrangements of functional groups that are common and essential to the biological activities of a set of high affinity ligands. The pharmacophore hypotheses can be validated in number of ways, including their ability to (i) rationalize the binding affinities of a training set of molecules of varying activity, (ii) successfully predict the affinities of a test set of molecules, and (iii) selectively retrieve known actives from a database of drug-like molecules [33].

A total of 135 molecules from three different scaffolds were used to generate a pharmacophore model having an activity range of 0.3 nM to 31.6 μM. The basic structures of the three different scaffolds are shown in Fig. 2. Activity less than or equal to 2 nM was considered active (8 molecules); activity greater than or equal to 340 nM was considered inactive (33 molecules). All the active molecules were used for generating a pharmacophore hypothesis. PHASE provides a maximum of 7 sites for pharmacophore generation, with features including hydrogen bond acceptors (A), hydrogen bond donors (D), hydrophobicity (H), aromatic rings (R), positively ionizable groups (P) and negatively ionizable groups (N). After applying default feature definitions to each ligand, common pharmacophores were generated using a terminal box the size of 1 Å and the requirement that all 8 actives should match. There were 30 hypotheses of 6 sites that survived the PHASE scoring procedure and matched the sites of all 8 active molecules. List of all 30 hypotheses with their scorings are depicted in supplementary data (Table S1). Though A, D, R, N and P pharmacophore features were used, all 30 hypotheses were devoid of negative and positive ionizable variables as it failed to match with the common sites of all 8 active molecules, Based on score actives and inactive, first 3 hypotheses (top 10%) were processed for generating QSAR modeling.

Table 2
Represents intersite distance in Å between pharmacophore features.

Site 1	Site 2	Distance (Å)
A1	A2	2.379
A1	D5	3.189
A1	R11	4.244
A1	R10	4.065
A1	R8	3.584
A2	D5	2.354
A2	R11	6.545
A2	R10	5.071
A2	R8	5.492
D5	R11	7.179
D5	R10	3.341
D5	R8	6.772
R11	R10	6.224
R11	R8	2.093
R10	R8	6.829

Equal numbers of molecules were divided randomly into the training and the test set, and partial least square statistical analysis was applied. The training and test set molecules were kept constant for the evaluation of pharmacophore hypotheses. Training and test sets consist of equal proportions of active, moderately active and inactive molecules with most active and most inactive molecule belonging to the training set. Up to 5 PLS factors were used to build a model for 68 training set molecules. Based on statistics, the best hypothesis out of 3 was considered for database screening. Regression statistics are shown in Table 4. A hypothesis was selected based on statistical values of r^2, r^2cv, Q^2, Pearson-R, F-value, P-value, standard deviation (SD), and root mean square error (RMSE) at the 5th PLS factor. The criteria of r^2 [34] and Q^2 [35] were utilized for the selection of the 5th PLS factor statistic. Cross validation of the model was performed by leave 20% out method, denoted as r^2cv. Based on scoring and statistic, AADRRR hypothesis was utilized for screening of database. The most predictive QSAR model was found to be associated with the six point hypothesis: two H-bond acceptors, one H-bond donor and three aromatic rings, denoted as AADRRR. The distance and angles between pharmacophore intersites is depicted in Fig. 3, Tables 2 and 3. The predicted activities of dataset molecules are shown in Table 1. A scatter plot of the training set and the predicted test set is shown in Fig. 4. In the training dataset, if the predicted value of a molecule was found to be ≥2 SD (0.8), it was considered an outlier [36]. There were 3 outliers found in the training dataset and discarded from the study.

A pharmacophore should generally contain 3 features, and it may not have more than 4 features [37], as reflected in the present study. There were several inhibitor molecules co-crystallized with the protein crystal structures that also contained 3 pharmacophoric features. Dessalew and co workers [38] have studied known inhibitor molecules that have co crystallized with protein crystals and found common features resembling the present AADRRR pharmacophore model. A study by Kim and co workers [39] found novel GSK-3β inhibitors using 3 validated pharmacophore models of 5 sites of AADHR, AAADH and AAADR. In the present study, a pharmacophore with 6 sites was found to correlate with the abovementioned models.

The most active (compound 16) and the most inactive (compound 46) molecules of the training set were overlapped with hypothesis to check the alignment and difference between the compounds (Figs. 5a and 6a). Basic nucleus and structure difference between them is shown in Fig. 2a. The most active molecule (basic scaffold: Fig. 2a1) was found well overlapped with hypothesis. In contrast, a fused ring of pyrazolo[1,5-b]pyridazine (basic scaffold: Fig. 2a3) of most inactive molecule distorted from the R8 and R11 of the hypothesis. Figs. 5b and 6b represent the favorable (green cubes) and non-favorable (violet cubes) region map
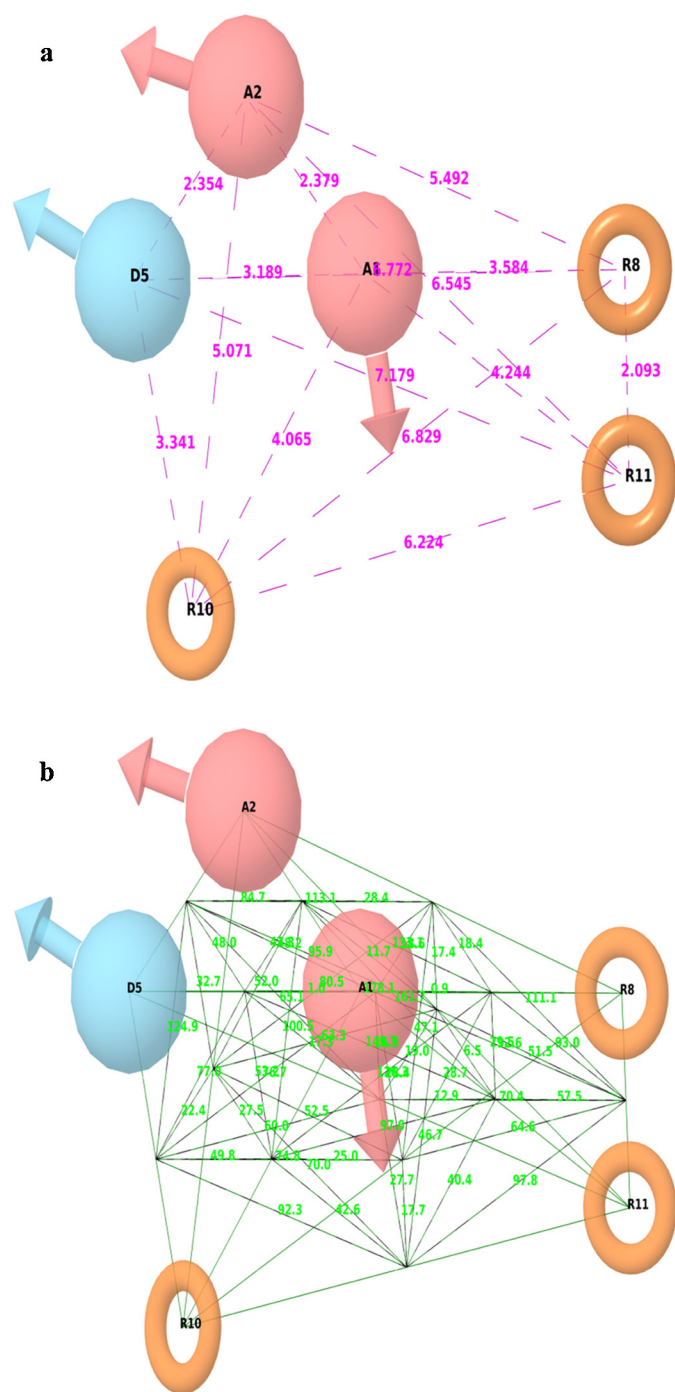
Fig. 3. The pharmacophore hypothesis (AADRRR) generated using the PHASE module. Intersite distances (a) are expressed in Angstroms. Intersite angles (b) are expressed in degrees. A: hydrogen bond acceptor; D: hydrogen bond donor; R: aromatic ring.

Table 3
Represents intersite angle in degree between pharmacophore features.

Site 1	Site 2	Site 3	Angle
A2	A1	D5	47.3
A2	A1	R11	161.7
A2	A1	R10	100.5
A2	A1	R8	133.1
D5	A1	R11	149.7
D5	A1	R10	53.2
D5	A1	R8	178.1
R11	A1	R10	97
R11	A1	R8	29.5
R10	A1	R8	126.3
A1	A2	D5	84.7
A1	A2	R11	11.7
A1	A2	R10	52
A1	A2	R8	28.4
D5	A2	R11	95.9
D5	A2	R10	32.7
D5	A2	R8	113.1
R11	A2	R10	63.3
R11	A2	R8	17.4
R10	A2	R8	80.5
A1	D5	A2	48
A1	D5	R11	17.3
A1	D5	R10	77
A1	D5	R8	1
A2	D5	R11	65.1
A2	D5	R10	124.9
A2	D5	R8	48.2
R11	D5	R10	60
R11	D5	R8	16.9
R10	D5	R8	76.7
A1	R11	A2	6.5
A1	R11	D5	12.9
A1	R11	R10	40.4
A1	R11	R8	57.5
A2	R11	D5	19
A2	R11	R10	46.7
A2	R11	R8	51.5
D5	R11	R10	27.7
D5	R11	R8	70.4
R10	R11	R8	97.8
A1	R10	A2	27.5
A1	R10	D5	49.8
A1	R10	R11	42.6
A1	R10	R8	25
A2	R10	D5	22.4
A2	R10	R11	70
A2	R10	R8	52.5
D5	R10	R11	92.3
D5	R10	R8	74.8
R11	R10	R8	17.7
A1	R8	A2	18.4
A1	R8	D5	0.9
A1	R8	R11	93
A1	R8	R10	28.7
A2	R8	D5	18.6
A2	R8	R11	111.1
A2	R8	R10	47.1
D5	R8	R11	92.6
D5	R8	R10	28.4
R11	R8	R10	64.6

Table 4
Showing statistical details of the pharmacophore hypothesis (AADRRR-35) after removal of outliers and including leave 20% out cross validation. PLS (partial least square), SD (standard deviation), r^2 (regression coefficient), r^2cv, F-value (Fisher value), RMSE (root mean square error), P-value (probability value), Q^2 (cross validation coefficient), and Pearson-R (Pearson regression).

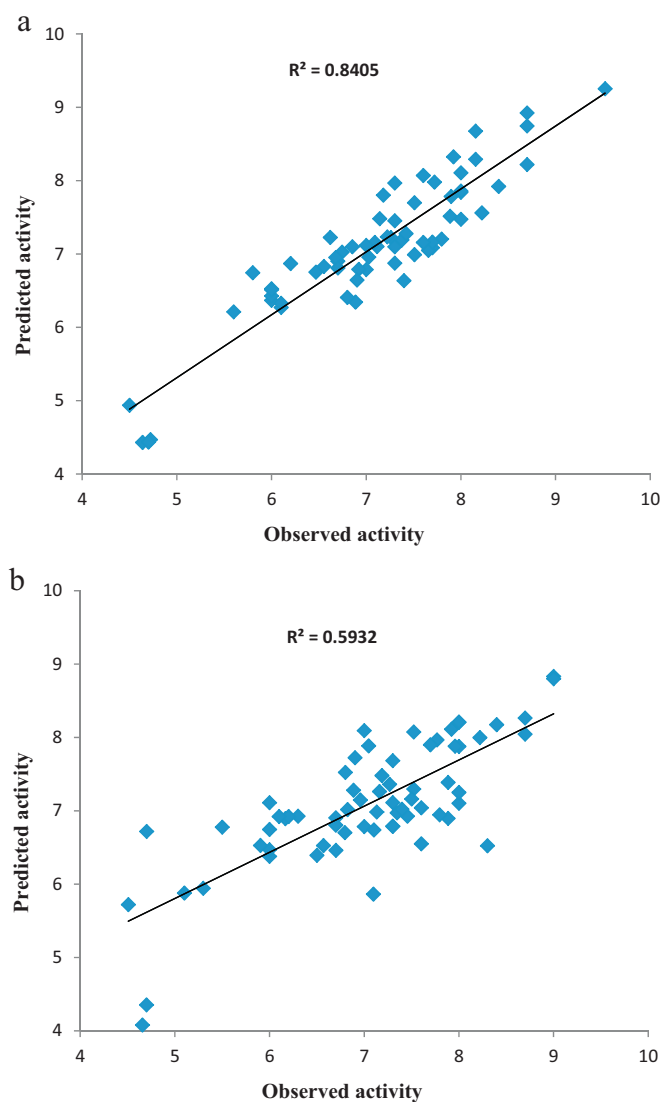| PLS factor	SD	r^2	r^2cv (L20%O)	F-value	RMSE	P-value	Q^2	Pearson-R
1	0.8	0.3772	0.2489	38.2	0.91	5.28×10^{-8}	0.2115	0.4772
2	0.6815	0.5554	0.3133	38.7	0.9	1.23×10^{-11}	0.2411	0.5327
3	0.544	0.7213	0.4674	52.6	0.84	6.46×10^{-17}	0.3423	0.6143
4	0.48	0.768	0.513	49.6	0.80	2.23×10^{-18}	0.4633	0.6619
5	0.41	0.8405	0.6644	49.4	0.72	7.63×10^{-20}	0.5932	0.7181

a

a

b

Fig. 4. A scatter plot of observed *vs.* predicted IC$_{50}$ values of the training set molecules (a) and the test set molecules (b).
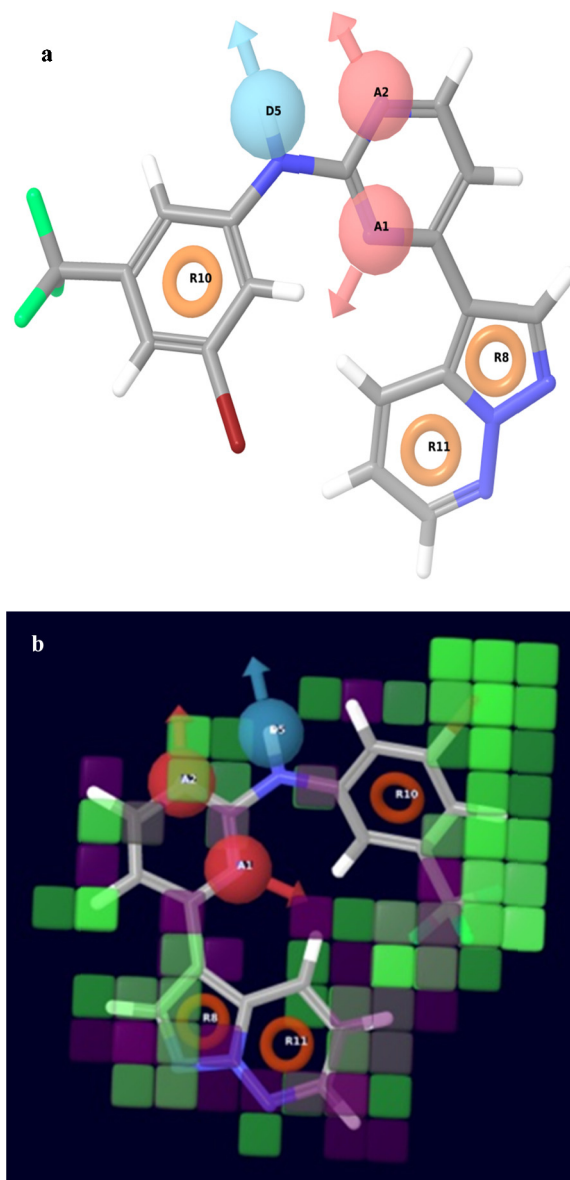
Fig. 5. The pharmacophore hypothesis alignment (a) and atom-based pharmacophore model representation (b), in context of the most active molecule. In section (a) pink sphere: A – hydrogen bond acceptor; blue sphere: D – hydrogen bond donor; orange torus: aromatic ring. In section (b) green cubes indicate positive coefficient (increase in activity), violet cubes indicate negative coefficient (decrease in activity). (For interpretation of the references to color in this figure legend, the reader is referred to the web version of the article.)

for the most active and inactive molecules, respectively. The color of the cube denotes favorable regions containing atoms or pharmacophore sites that favor the biological activity. Better predicted activity is assumed if the predominance of favorable regions for the molecule. The most active molecule (compound 16) from the training set which was overlapped well to the hypothesis and observed that the only two nitrogen atoms in the fused aromatic ring were non-favorable, which is not a part of pharmacophore feature. The functional group −Br and −CF$_3$ at 3rd and 5th position may enhance the hydrophobic and electrostatic interactions. On the other hand, the most inactive molecule (compound 46) which was distorted from the hypothesis, showed all the pharmacophore sites are non favorable except one acceptor (−N) atom. The reason for the poor predictability for the most inactive molecule, though most active and inactive molecules were belongs to the same scaffold, may be due to the presence of bulkier and hydrophobic 4-methoxy phenyl functional group at the 2nd position of the pyrazolo[1,5-b]pyridazine nucleus. 4-Methoxy phenyl functional group imparting excess hydrophobicity compared to the most active molecule, may be responsible for inactivity. In order to gain more insight in to the predictability of these molecules, docking was

performed between most active and inactive molecules with GSK-3β (1Q5K). Docked pose is shown in Fig. 7. The most active molecule was colored purple and the most inactive molecule was colored green. The most active molecule was found occupying active site with 2-H bond interactions whereas, the most inactive molecule skipped out from the active site, labeled as umbrella effect and there were no interaction found with protein. Presence of strong hydrophobic p-methoxy phenyl functional group, lacking of small hydrophobic bromine functional group and docking observation highlighted that the electrostatic and hydrophobic halide atoms particularly to 3rd and 5th position, may favor the biological activity and excess hydrophobicity may be non-favorable.

3.2. Database screening

There were over 200,000 molecules existing in database and used to find hits. Ligand preparation was performed on all database
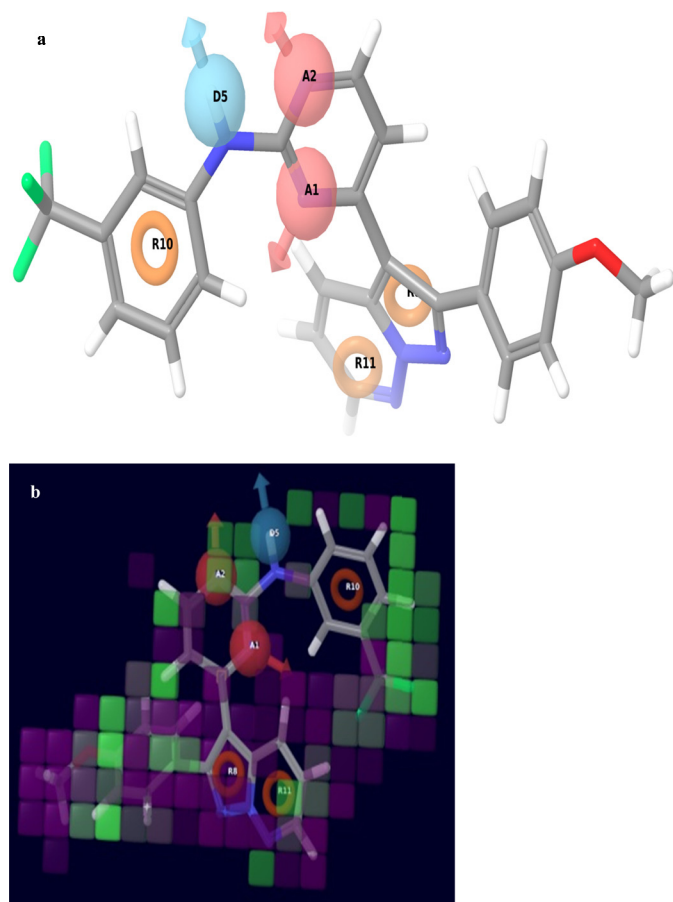
Fig. 6. The pharmacophore hypothesis alignment (a) and atom-based pharmacophore model representation (b), in context of the most inactive molecule. In section (a) pink sphere: A – hydrogen bond acceptor; blue sphere: D – hydrogen bond donor; orange torus: aromatic ring. In section (b) green cubes indicate positive coefficient (increase in activity), violet cubes indicate negative coefficient (decrease in activity). (For interpretation of the references to color in this figure legend, the reader is referred to the web version of the article.)
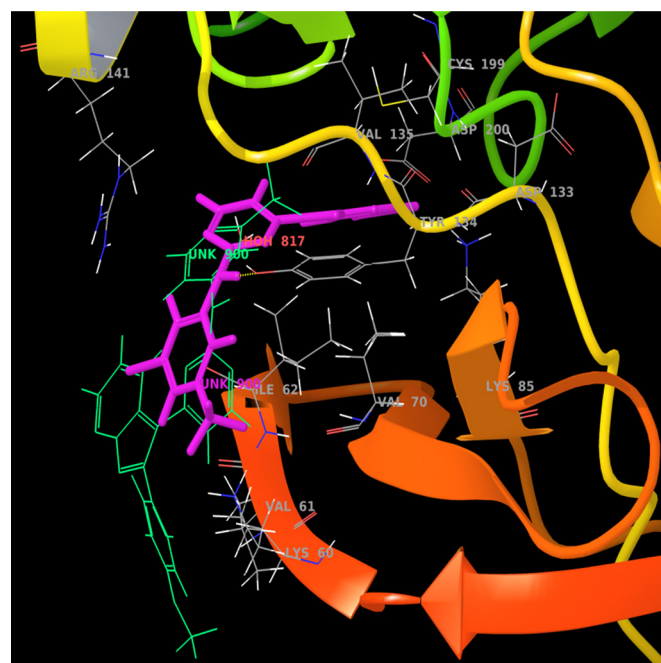

Fig. 7. Showing docked pose of the most active and the most inactive molecules of database with GSK-3β (PDB ID: 1Q5K). The most active molecule colored purple and the most inactive colored green. (For interpretation of the references to color in this figure legend, the reader is referred to the web version of the article.)

molecules. Through the advanced pharmacophore search module in Schrödinger, all the prepared ligands were screened through the pharmacophore hypothesis. The criteria of relative energy window, rotatable bonds, intersite distance matching tolerance and number of pharmacophore site matched were considered for screening of database to retrieve primary hits. The cut off values of relative energy window was kept 10 kcal/mol, rotatable bond of a confirmer should be <10, intersite distance matching tolerance of 2 Å with all the pharmacophore sites must match. Through this screening, 357 primary hits were found to match the pharmacophore model and were subsequently ranked by their phase predicted activity.

3.3. Docking study

The current study employs a structure-based approach to narrow down the primary hits by means of docking score and ligand protein interactions. GSK-3β (PDB ID: 1Q5K) and CDK5 (PDB ID: 1UNL) proteins were used to identify the molecules selective to GSK-3β form the primary hits. Validation of the binding site and extraction of key amino acid residues were accomplished by docking ATP and the respective reference standard molecules with GSK-3β and CDK5. Protein validation was achieved by calculating RMSD values between the atom sets of the native X-ray pose and the top ranked docked pose.

Because this study focused on ATP competitive inhibitors, the ATP binding site and important interactions in GSK-3β and CDK5

need to be confirmed to achieve selectivity for GSK-3β. For protein validation and confirmation of the ATP binding site, ATP and the reference standard molecules were docked to the protein crystal structure. The docked pose of ATP in GSK-3β and in CDK5 is shown in the supplementary data (Figures S2b and S3b). Docking analysis revealed that H-bonds, ionic and hydrophobic interactions were observed between ATP and Asp133, Tyr134, Val135, Pro136 and Arg141 of GSK-3β. Similarly Glu81, Asp86, Lys128, Gln130 and Asn144 in CDK5/p25 were observed to interact with ATP.

Second strategy was applied to both proteins for validation, wherein RMSD was calculated between atom set of the reference standard molecules of the native X-ray pose and the best pose obtained after docking with the respective protein crystal structure. Native X-ray crystal and docked pose was superimposed and interactions were depicted in Fig. 8 for both proteins. The molecule colored purple belongs to the native X-ray crystal and colored green belongs to the best dock pose for both the proteins. Both of them superimposed well and RMSD was found 0.7460 Å for 1Q5K and 0.5779 Å for 1UNL. For both the reference standard molecules, the RMSD was found less than 1 Å [40] and showed 100% similarity in amino acid interactions. Ligand–protein interaction of AR-A 014418 with 1Q5K protein and R-roscovitine with 1UNL protein are shown in supplementary data (Figures S2a and S3a).

There are 3 well characterized regions in the ATP binding pocket of GSK-3β that are responsible for the inhibitory activity of molecules, and these regions are (i) hinge region residues – Asp133, Tyr134 and Val135, (ii) a hydrophobic pocket – Ile62, Gly63, Phe67 and Val70 and (iii) a polar region – Lys85, Glu97, Arg141, Glu185, Cys199 and Asp200. Interaction with amino acid residues of any two regions is necessary for selectivity as well as inhibitory activity [45]. Interaction with hinge region residues is important for potency for GSK-3β inhibition. Interaction with the polar region and/or the hydrophobic pocket region determines selectivity as well as potency for GSK-3β. A review of ligand–protein interaction reveals that Asp133, Val135, Glu137, Arg141, Gln185, Asp200 and Arg220 show prominent interaction with known potent and selective inhibitors [41–45]. For GSK-3β, Asp133 and Val135 (Glu81
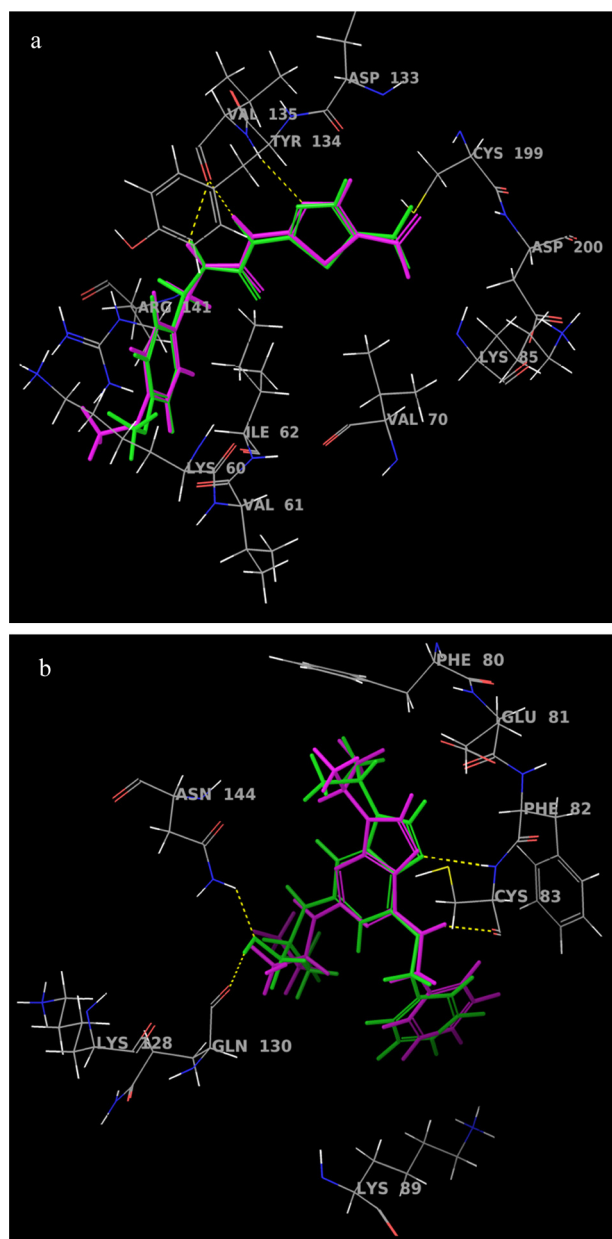
Fig. 8. Representing superimposition of native X-ray crystal and the best docked pose of a reference standard AR-A 014418 with GSK-3β (PDB ID: 1Q5K) (a) and R-roscovitine with CDK5 (PDB ID: 1UNL) (b). In figure the molecule colored purple belongs to the native X-ray crystal and colored green belongs to the best dock pose for both the proteins. (For interpretation of the references to color in this figure legend, the reader is referred to the web version of the article.)

Table 5
Showing the inhibitory concentrations of selected molecules from the SPECS database for GSK-3β and CDK5 proteins; their identity codes and fold selectivity for GSK-3β are indicated.

No.	SPECS ID	IC$_{50}$ values (μM)		Fold selectivity to GSK-3β
		GSK-3β	CDK5/p25	
1	AE-848/11244036	0.927	36.7	39
2	AN-648/41666070	1.116	64.3	57
3	AJ-292/14925154	0.825	27.9	33
4	AA-516/30011006	0.983	22.8	23
5	AE-848/08054010	0.861	27.6	32

predicted activity and XP glide score parameters were included as a selection criteria. The molecules having phase predicted activity ≥8.0 and XP glide score ≥−8.0 for GSK-3β and ≤−6.0 for CDK5 were selected. The docked poses of primary hits after docking were carefully observed for their interaction with amino acid residues and docking scores for GSK-3β and CDK5. Finally, 5 hits were isolated that showed selective interactions with GSK-3β. Inhibitory concentration of these selected molecules is depicted in Table 5. The docked poses of these 5 hits in 1Q5K and 1UNL are shown in Figs. 9 and 10, and the detailed interactions are summarized in Table 6. The structures of these 5 molecules are shown in Fig. 11.

Molecule 1 comprises two basic scaffolds, namely imidazo-isoquinoline and benzimidazole. The former one showed H-bond with hydrophobic amino acid residue and π-cationic interaction that was absent in CDK5. The benzimidazole scaffold strongly occupied in the hydrophobic cavity of GSK-3β formed by Val61, Ile62, Gly63, Phe67 and Val70 and made hydrophobic interaction. The volume of ATP binding pocket in CDK5 is smaller than that in GSK-3β, enabling the latter protein to hold an imidazo-isoquinoline scaffold, making a reorientation of the molecule from the ATP binding site of CDK5. Of all the molecules, molecule 2 was the most flexible and had an anionic carboxylate group that could easily reorient in binding pocket with electrostatic interaction, favored ionic interaction with GSK-3β but not with CDK5. The amide linker oriented parallel to the hinge region in GSK-3β that formed 2H-bonds which was not observed in CDK5. The keto functional group and sulphur atom of the thiazolidinedione favored H-bonding and small atom hydrophobicity to GSK-3β. There was involvement of hinge region residues, electropositive Arg141 (molecule 1), hydrophobic Val61 (molecule 1) and electropositive Lys60 (molecule 2) residues in GSK-3β. These interactions showed hydrophobically packed H-bond, ionic, electrostatic interaction and small atom hydrophobicity along with reorientation of molecules 1 and 2 from binding pocket of CDK5 made these molecules selective over CDK5.

In molecule 3, N7 of purine showed a typical H-bond interaction with the DFG motif (activation loop) of GSK-3β. The purine ring fits in the polar region formed by Lys85, Glu97, Glu185 and Asp200 and differs in CDK5. There was π-cationic interaction observed of purine in CDK5. Amide functional group of benzamide showed a similar type of interaction both with GSK-3β and CDK5. Though molecule 3 showed similar interactions, the only differentiating interaction was with Asp200 in GSK-3β, which may explain the selectivity for GSK-3β.

Benzothiophene scaffold of molecule 4 possess hydrophobic chlorine atom at 5th position that oriented in a hydrophobic pocket of GSK-3β, possessed π-cationic and small atom hydrophobic interaction, allowing selectivity. In molecule 5, the aromatic ring of p-toluene sulphonic acid showed π-cationic interaction with Arg141 and the hydrazide linker between the indole and benzene-sulphonic acid interacted with water by 2H-bonds, which were lacking in CDK5. The interaction of molecule 5 with Asp133, Arg141
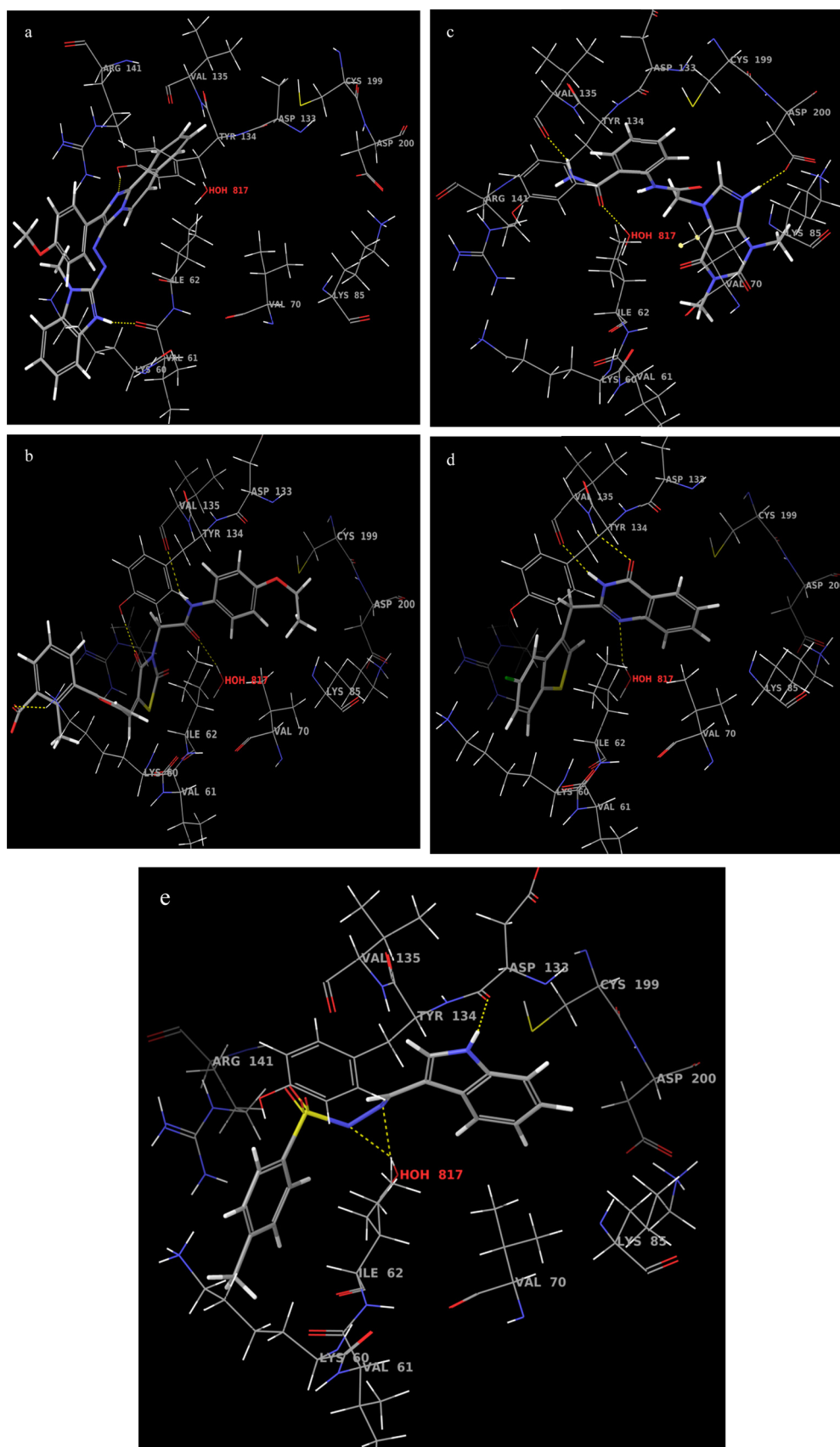
and Cys83 for CDK5) are the most prominent for binding characteristics beneath the hinge region and form 1–3 H-bonds with ATP competitive ligands [30,46]. Apart from these residues, Tyr134 (Phe82 for CDK5) imparts a hydrophobic interaction and Arg141 (Lys89 in CDK5) contributes an ionic or π-cationic interaction with a molecule that fits in a hydrophobic pocket formed by the gatekeeper residue Leu132 (Phe80 in CDK5).

The molecules were selected from the primary hits by considering phase predicted activity, glide score and key interactions with proteins. Molecules that showing minimum of 2 interactions with Asp133, Val135, Tyr134 (hinge region) and Arg141 amino acid residues of GSK-3β and should have least H-bond interactions with Cys83, Glu81 and Gln130 amino acid residues of CDK5 were selected. Along with above mentioned interaction constrain, phase

Fig. 9. Representation of the ligand interaction with GSK-3β protein (PDB ID: 1Q5K) for molecule 1 – AE-848/11244036 (a), molecule 2 – AN-648/41666070 (b), molecule 3 – AJ-292/14925154 (c), molecule 4 – AA-516/30011006 (d) and molecule 5 – AE-848/08054010 (e), which were hits from the SPECS database.
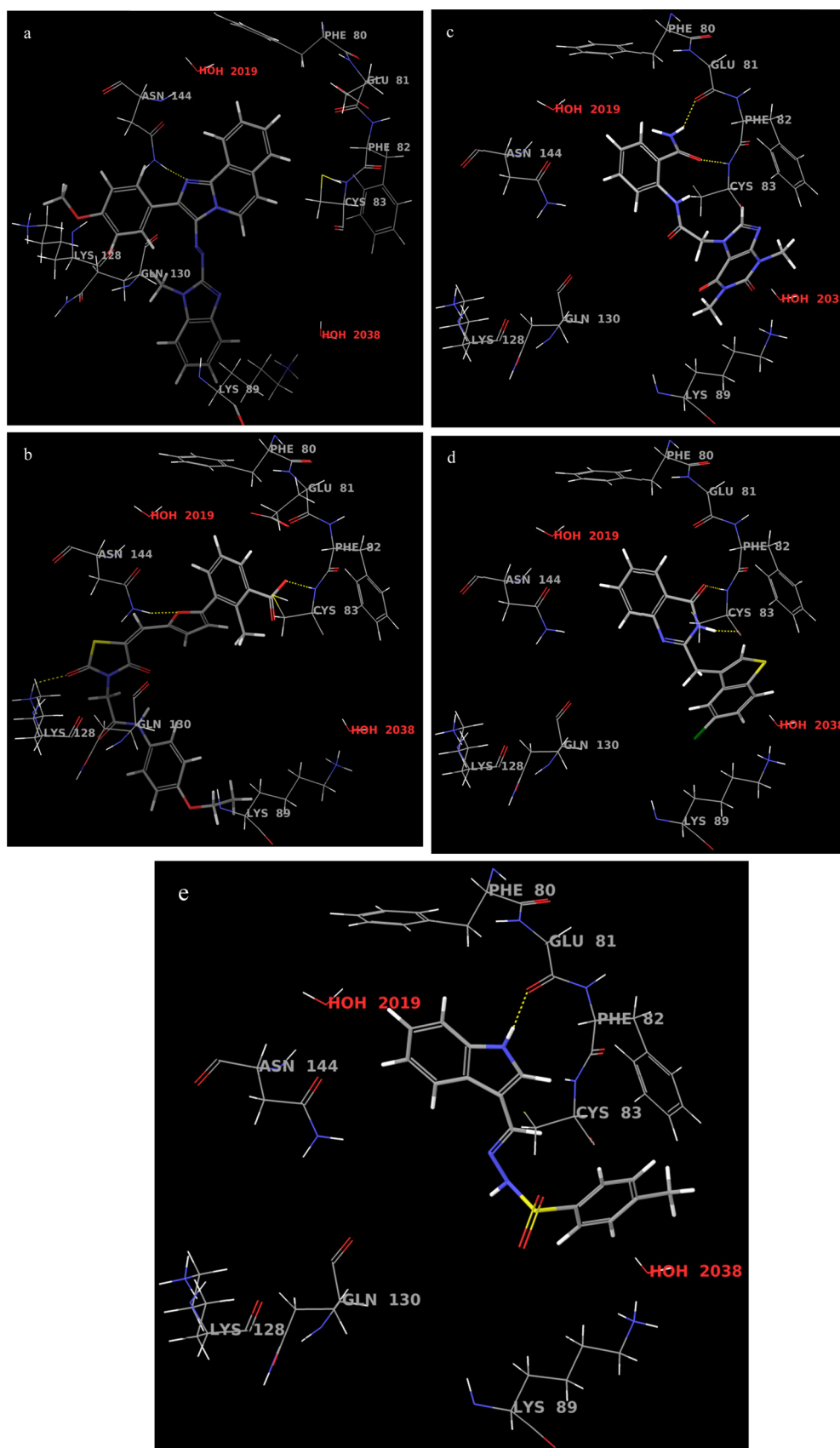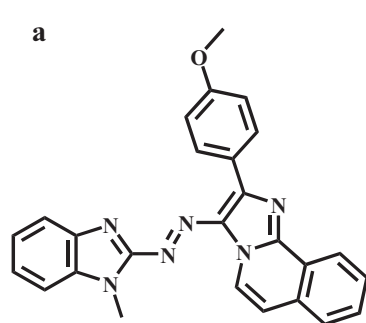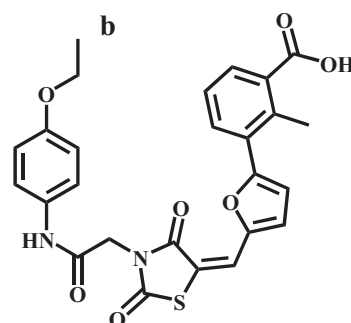
Fig. 10. Showing ligand interactions with CDK5 protein (PDB ID: 1UNL) for molecule 1 – AE-848/11244036 (a), molecule 2 – AN-648/41666070 (b), molecule 3 – AJ-292/14925154 (c), molecule 4 – AA-516/30011006 (d) and molecule 5 – AE-848/08054010 (e), which were hits from the SPECS database.

Table 6
Illustrating the detailed interactions of ligands with both GSK-3β (PDB ID: 1Q5K) and CDK5 (PDB ID: 1UNL).

No.	Scaffold name	Interaction with 1Q5K (GSK-3β)		Interaction with 1UNL (CDK5)	
		Amino acid residues involved	Type of interaction	Amino acid residues involved	Type of interaction
1	Imidazo-isoquinoline	Tyr134 (Side chain with -OH)	1 hydrogen bond	Asn144 (carbonyl backbone)	1 Hydrogen bond
		Arg141 (charged amino group)	π-Cationic		
	Benzimidazole	Val61 (carbonyl backbone)	1 Hydrogen bond		
2	Thiazolidinedione derivative	Lys60 (charged amino group)	Ionic	Cys83 (amide backbone)	1 Hydrogen bond
		Tyr134 (Side chain with -OH)	1 hydrogen bond	Asn144 (amide backbone)	1 Hydrogen bond
		Val135 (carbonyl backbone)	1 hydrogen bond	Lys128 (amide side chain)	1 hydrogen bond
		H_2O	1 hydrogen bond		
3	Purine	Asp200 (Side chain with —OH)	1 hydrogen bond	Phe82	Hydrophobic
	Benzamide	Val135 (carbonyl backbone)	1 hydrogen bond	Glu81 (carbonyl backbone)	1 hydrogen bond
		H_2O	2 hydrogen bond	Cys83 (amide backbone)	1 hydrogen bond
4	Quinazolinone	Val135 (carbonyl and amide backbone)	2 hydrogen bond	Cys83 (carbonyl and amide backbone)	2 hydrogen bond
		Arg141 (charged amino group)	π-Cationic	Lys89 (charged amino group)	π-Cationic
	Benzothiophene	H_2O	1 hydrogen bond		
5	1H-Indole	Asp133 (carbonyl backbone)	1 hydrogen bond	Phe82	Hydrophobic
	Benzene sulphonic acid	Arg141 (charged amino group)	π-Cationic	Glu81 (carbonyl backbone)	1 hydrogen bond
		H_2O	2 hydrogen bond		
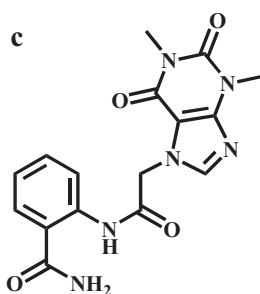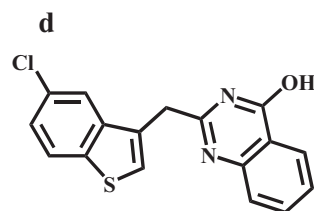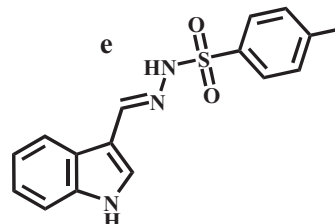
Fig. 11. Denoting the structure of 5 selected molecules, namely molecule 1 – AE-848/11244036 (a), molecule 2 – AN-648/41666070 (b), molecule 3 – AJ-292/14925154 (c), molecule 4 – AA-516/30011006 (d) and molecule 5 – AE-848/08054010 (e) from the SPECS database.

and a water molecule may explain the selectivity of this molecule for GSK-3β.

According to ligand–protein interaction and *in vitro* kinase inhibition assay data, purine, thiazolidinedione and imidazo-isoquinoline scaffolds represent interesting compounds for further exploration. The purine derivative (molecule 3) was found to be the most potent and selective. A thiazolidinedione scaffold (molecule 2) could be explored further, as it was found to be the most selective (57 fold) to GSK-3β. The imidazo-isoquinoline scaffold (molecule 1) could generate novel series of inhibitors and is expected to have high affinity, due to hydrophobic contacts along with ionic interactions holding if firmly in the active site of GSK-3β. The above mentioned scaffolds showed interaction with critical amino acid residues critical for selectivity.

4. Conclusion

Combined LBDD and SBDD approaches identified 5 hits having isoquinoline, thiazolidinedione, purine, quinazolinone and benzothiophene scaffolds. These hits showed IC_{50} values ranging from 0.825 μM to 1.116 μM and were 23–57-fold selective for GSK-3β. These inhibitory potencies were confirmed by an enzyme inhibition assay. Lys60, Val61, Arg141 and Asp200 were believed to favor selectivity for GSK-3β over CDK5. Asp133, Tyr134 and Val135 were important for potency. Molecule 3, a purine analog, was found to have the lowest IC_{50} value, 0.825 μM, of all the active compounds. Our research highlighted molecules possessing benzothiophene, isoquinoline, thiazolidinedione imidazo-isoquinoline and quinazolinone scaffolds. Docking analysis of energy-minimized conformations of these selective molecules showed small atom hydrophobicity and ionic or π-cationic interactions, which were further strengthened by H-bonding with important amino acid residues and a water molecule.

Future direction

The 5 selected hits could also be used in *in vitro* and *in vivo* studies to evaluate their neuroprotective potential. Future experiments could focus this research on optimizing these 5 leads for better potency and selectivity toward GSK-3β.

Conflicts of interest

The authors report no declarations of interest.

Acknowledgements

Appendix A. Supplementary data

Supplementary material related to this article can be found, in the online version, at http://dx.doi.org/10.1016/j.jmgm.2014.06.013.

References

[1] J.R. Woodgett, Molecular cloning and expression of glycogen synthase kinase-3/factor A, EMBO J. 9 (1990) 2431–2438.

[2] M. Takahashi, K. Tomizawa, R. Kato, K. Sato, T. Uchida, S.C. Fujita, K. Imahori, Localization and developmental changes of tau protein kinase I/glycogen synthase kinase-3 beta in rat brain, J. Neurochem. 63 (1994) 245–255.

[3] G.N. Bijur, R.S. Jope, Glycogen synthase kinase-3 beta is highly activated in nuclei and mitochondria, Neuroreport 14 (2003) 2415–2419.

[4] K. Hughes, E. Nikolakaki, S.E. Plyte, N.F. Totty, J.R. Woodgett, Modulation of the glycogen synthase kinase-3 family by tyrosine phosphorylation, EMBO J. 12 (1993) 803–808.

[5] C. Picton, J. Woodgett, B. Hemmings, P. Cohen, Multisite phosphorylation of glycogen synthase from rabbit skeletal muscle: phosphorylation of site 5 by glycogen synthase kinase-5 (casein kinase-II) is a prerequisite for phosphorylation of sites 3 by glycogen synthase kinase-3, FEBS Lett. 150 (1982) 191–196.

[6] A. Kannoji, S. Phukan, V. Sudher Babu, V.N. Balaji, GSK3beta: a master switch and a promising target, Expert Opin. Ther. Targets 12 (2008) 1443–1455.

[7] M.P. Mazanetz, P.M. Fischer, Untangling tau hyperphosphorylation in drug design for neurodegenerative diseases, Nat. Rev. Drug Discov. 6 (2007) 464–479.

[8] D. Tang, J.H. Wang, Cyclin-dependent kinase 5 (Cdk5) and neuron-specific Cdk5 activators, Prog. Cell Cycle Res. 2 (1996) 205–216.

[9] S. Cicero, K. Herrup, Cyclin-dependent kinase 5 is essential for neuronal cell cycle arrest and differentiation, J. Neurosci. 25 (2005) 9658–9668.

[10] F. Causeret, T. Jacobs, M. Terao, O. Heath, M. Hoshino, N. Nikolic, Neurabin-I is phosphorylated by Cdk5: implications for neuronal morphogenesis and cortical migration, Mol. Biol. Cell 18 (2007) 4327–4342.

[11] T. Ohshima, E.C. Gilmore, G. Longenecker, D.M. Jacobowitz, R.O. Brady, K. Herrup, A.B. Kulkarni, Migration defects of cdk5(−/−) neurons in the developing cerebellum is cell autonomous, J. Neurosci. 19 (1999) 6017–6026.

[12] V. Stambolic, L. Ruel, J.R. Woodgett, Lithium inhibits glycogen synthase kinase-3 activity and mimics wingless signalling in intact cells, Curr. Biol. 6 (1996) 1664–1668.

[13] L. Meijer, M. Flajolet, P. Greengard, Pharmacological inhibitors of glycogen synthase kinase 3, Trends Pharmacol. Sci. 25 (2004) 471–480.

[14] A. Martinez, M. Alonso, A. Castro, C. Pérez, F.J. Moreno, First non-ATP competitive glycogen synthase kinase 3 beta (GSK-3beta) inhibitors: thiadiazolidinones (TDZD) as potential drugs for the treatment of Alzheimer's disease, J. Med. Chem. 45 (2002) 1292–1299.

[15] M. Hamann, D. Alonso, E. Martín-Aparicio, A. Fuertes, M.J. Pérez-Puerto, A. Castro, S. Morales, M.L. Navarro, M. Del Monte-Millán, M. Medina, A. Pennaka, A. Balaiah, J. Peng, J. Cook, S. Wahyuono, A. Martínez, Glycogen synthase kinase-3 (GSK-3) inhibitory activity and structure–activity relationship (SAR) studies of the manzamine alkaloids. Potential for Alzheimer's disease, J. Nat. Prod. 70 (2007) 1397–1405.

[16] S. Conde, D.I. Pérez, A. Martínez, C. Perez, F.J. Moreno, Thienyl and phenyl alpha-halomethyl ketones: new inhibitors of glycogen synthase kinase (GSK-3beta) from a library of compound searching, J. Med. Chem. 46 (2003) 4631–4633.

[17] S. Phukan, V.S. Babu, A. Kannoji, R. Hariharan, V.N. Balaji, GSK3beta: role in therapeutic landscape and development of modulators, Br. J. Pharmacol. 160 (2010) 1–19.

[18] D. Wei, X. Jiang, L. Zhou, J. Chen, Z. Chen, C. He, K. Yang, Y. Liu, J. Pei, L. Lai, Discovery of multitarget inhibitors by combining molecular docking with common pharmacophore matching, J. Med. Chem. 51 (2008) 7882–7888.

[19] S.H. Lu, J.W. Wu, H.L. Liu, J.H. Zhao, K.T. Liu, C.K. Chuang, H.Y. Lin, W.B. Tsai, Y. Ho, The discovery of potential acetylcholinesterase inhibitors: a combination of pharmacophore modeling, virtual screening, and molecular docking studies, J. Biomed. Sci. 18 (2011) 8–20.

[20] F.X. Tavares, J.A. Boucheron, S.H. Dickerson, R.J. Griffin, F. Preugschat, S.A. Thomson, T.Y. Wang, H.Q. Zhou, N-phenyl-4-pyrazolo[1,5-b]pyridazin-3-ylpyrimidin-2-amines as potent and selective inhibitors of glycogen synthase kinase 3 with good cellular efficacy, J. Med. Chem. 47 (2004) 4716–4730.

[21] P. Polychronopoulos, P. Magiatis, A.L. Skaltsounis, V. Myrianthopoulos, E. Mikros, A. Tarricone, A. Musacchio, S.M. Roe, L. Pearl, M. Leost, P. Greengard, L. Meijer, Structural basis for the synthesis of indirubins as potent and selective inhibitors of glycogen synthase kinase-3 and cyclin-dependent kinases, J. Med. Chem. 47 (2004) 935–946.

[22] M. Saitoh, J. Kunitomo, E. Kimura, H. Iwashita, Y. Uno, T. Onishi, N. Uchiyama, T. Kawamoto, T. Tanaka, C.D. Mol, D.R. Dougan, G.P. Textor, G.P. Snell, M. Takizawa, F. Itoh, M. Kori, 2-{3-[4-(Alkylsulfinyl)phenyl]-1-benzofuran-5-yl}-5-methyl-1,3,4-oxadiazole derivatives as novel inhibitors of glycogen synthase kinase-3beta with good brain permeability, J. Med. Chem. 52 (2009) 6270–6286.

[23] Maestro, Version 9.0, Schrödinger, LLC, New York, NY, 2010.

[24] LigPrep, Version 2.3, Schrödinger, LLC, New York, NY, 2010.

[25] U.A. Shah, H.S. Deokar, S.S. Kadam, V.M. Kulkarni, Pharmacophore generation and atom-based 3D-QSAR of novel 2-(4-methylsulfonylphenyl)pyrimidines as COX-2 inhibitors, Mol. Divers. 14 (2010) 559–568.

[26] Y. Li, Y. Wang, F. Zhang, Pharmacophore modeling and 3D-QSAR analysis of phosphoinositide 3-kinase p110alpha inhibitors, J. Mol. Model. 16 (2010) 1449–1460.

[27] Phase, Version 3.2, Schrödinger, LLC, New York, NY, 2010.

[28] S.L. Dixon, A.M. Smondyrev, E.H. Knoll, S.N. Rao, D.E. Shaw, R.A. Friesner, PHASE: a new engine for pharmacophore perception, 3D QSAR model development, and 3D database screening: 1. Methodology and preliminary results, J. Comput. Aided Mol. Des. 20 (2006) 647–671.

[29] R. Bhat, Y. Xue, S. Berg, S. Hellberg, M. Ormö, Y. Nilsson, A.C. Radesäter, E. Jerning, P.O. Markgren, T. Borgegård, M. Nylöf, A. Giménez-Cassina, F. Hernández, J.J. Lucas, J. Díaz-Nido, J. Avila, Structural insights and biological effects of glycogen synthase kinase 3-specific inhibitor AR-A014418, J. Biol. Chem. 278 (2003) 45937–45945.

[30] M. Mapelli, L. Massimiliano, C. Crovace, M.A. Seeliger, L.H. Tsai, L. Meijer, A. Musacchio, Mechanism of CDK5/p25 binding by CDK inhibitors, J. Med. Chem. 48 (2005) 671–679.

[31] Glide, Version 5.6, Schrödinger, LLC, New York, NY, 2010.

[32] A. Baki, A. Bielik, L. Molnár, G. Szendrei, G.M. Keserü, A high throughput luminescent assay for glycogen synthase kinase-3beta inhibitors, Assay Drug Dev. Technol. 5 (2007) 75–83.

[33] S.L. Dixon, A.M. Smondyrev, S.N. Rao, PHASE: a novel approach to pharmacophore modeling and 3D database searching, Chem. Biol. Drug Des. 67 (2006) 370–372.

[34] R.P. Verma, C. Hansch, QSAR modeling of taxane analogues against colon cancer, Eur. J. Med. Chem. 45 (2010) 1470–1477.

[35] A. Golbraikh, A. Tropsha, Beware of q2!, J. Mol. Graph. Model. 20 (2002) 269–276.

[36] B. Balaji, R. Muthiah, R. Sabarinath, Chandrasekharan, Descriptor analysis of estrogen receptor β-selective ligands using 2-phenylquinoline, tetrahydrofluorenone and 3-hydroxy 6H-benzo[c]chromen-6-one scaffolds, J. Enzyme Inhib. Med. Chem. 26 (2011) 831–842.

[37] J.H. Van Drie, Pharmacophore discovery—lessons learned, Curr. Pharm. Des. 91 (2003) 649–1664.

[38] N. Dessalew, P.V. Bharatam, Identification of potential glycogen kinase-3 inhibitors by structure based virtual screening, Biophys. Chem. 128 (2007) 165–175.

[39] H.J. Kim, H. Choo, Y.S. Cho, K.T. No, A.N. Pae, Novel GSK-3beta inhibitors from sequential virtual screening, Bioorg. Med. Chem. 16 (2008) 636–643.

[40] D.I. Osolodkin, V.A. Palyulin, N.S. Zefirov, Structure-based virtual screening of glycogen synthase kinase 3β inhibitors: analysis of scoring functions applied to large true actives and decoy sets, Chem. Biol. Drug Des. 78 (2011) 378–390.

[41] L. Feng, Y. Geisselbrecht, S. Blanck, A. Wilbuer, G.E. Atilla-Gokcumen, P. Filippakopoulos, K. Kräling, M.A. Celik, K. Harms, J. Maksimoska, R. Marmorstein, G. Frenking, S. Knapp, L.O. Essen, E. Meggers, Structurally sophisticated octahedral metal complexes as highly selective protein kinase inhibitors, J. Am. Chem. Soc. 20 (2011) 5976–5986.

[42] C. Logé, A. Testard, V. Thiéry, O. Lozach, M. Blairvacq, J.M. Robert, L. Meijer, T. Besson, Novel 9-oxo-thiazolo[5,4-f]quinazoline-2-carbonitrile derivatives as dual cyclin-dependent kinase 1 (CDK1)/glycogen synthase kinase-3 (GSK-3) inhibitors: synthesis, biological evaluation and molecular modeling studies, Eur. J. Med. Chem. 43 (2008) 1469–1477.

[43] M. Arnost, A. Pierce, E. Haar, D. Lauffer, J. Madden, K. Tanner, J. Green, 3-Aryl-4-(arylhydrazono)-1H-pyrazol-5-ones: highly ligand efficient and potent inhibitors of GSK3beta, Bioorg. Med. Chem. Lett. 20 (2010) 1661–1664.

[44] V. Pande, M.J. Ramos, Structural basis for the GSK-3beta binding affinity and selectivity against CDK-2 of 1-(4-aminofurazan-3yl)-5-dialkylaminomethyl-1H-[1-3] triazole-4-carboxylic acid derivatives, Bioorg. Med. Chem. Lett. 15 (2005) 5129–5135.

[45] T. Kramer, B. Schmidt, F.L. Monte, Small-molecule inhibitors of GSK-3: structural insights and their application to Alzheimer's disease models, Int. J. Alzheimers Dis. 2012 (2012) 1–32.

[46] N. Zhang, Y.J. Jiang, Q.S. Yu, J.W. Zou, Studies of glycogen synthase kinase-3 inhibitors, Prog. Chem. 19 (2007) 614–623.